PCCP

Accepted Manuscript

ROYAL SOCIETY OF CHEMISTRY

www.rsc.org/pccp

Journal Name

ARTICLE

π-Topology and Spin Alignment in the Photo-Excited States of Phenylanthracene-*t*-Butylnitroxide Radicals

Received 00th January 20xx,
Accepted 00th January 20xx

DOI: 10.1039/x0xx00000x

www.rsc.org/

Yoshio Teki,[a]* Sadaharu Miyamoto,[a] and Kentaro Koide[a]

We have studied the relationship between the π-topology and the photo-excited high-spin states of π-conjugated spin systems, 9-anthracen-(3-phenyl-*t*-butylnitroxide) radical (**1*m***) and 9-anthracen-(4-phenyl-*t*-butylnitroxide) radical (**1*p***) by the time-resolved ESR and transient absorption spectroscopies. For the *meta*-isomer, **1*m***, the excited quartet high-spin state (S = 3/2) was observed, while for *para*-isomer, **1*p***, only a weak signal of the doublet state (S = 1/2) was detected. For the quartet state of **1*m***, the *g* value and fine-structure parameters have been determined to be g = 2.005, D = 0.0250 cm^{-1}, E = ~ 0.0 cm^{-1}. The mechanism of the intramolecular spin alignment and the role of the spin polarization on the excited states have been discussed based on the spin density distribution calculated by the *ab-initio* molecular orbital calculations.

Introduction

Intramolecular spin alignment and exchange interaction through π-conjugation in purely organic spin systems are quite important in the field of molecule-based magnetism [1] and organic spintronics [2]. Recently, a possibility of organic radical based spintronics was also demonstrated by T. Sugawara et al.[3]. Most of these studies are limited to ground state systems. The studies on the relationship between the π-topology and the metastable excited state will give very important issue on the forthcoming excited-state organic spintronics as well as the photo-control of the magnetic properties [4]. Thus, this knowledge leads to a new strategy for the photo-induced/switching magnetic spin systems, the photo-control of the molecule-based magnetism [5] and future organic spintronics devices using light excitation. π-Conjugated spin systems constructed from the condensed polynuclear aromatic hydrocarbons (anthracene, pyrene, pentacene and so forth) and the covalently-linked stable radicals are ideal model systems in order to study the relationship between the π-topology and photoinduced spin alignment. The spin correlation of their unpaired electrons via the delocalized π orbital network is most important for determining the spin states in the photo-excited states as well as the electronic ground state.

In this paper, we describe the intramolecular spin alignment and the role of the spin correlation on the spin alignment in the excited spin states of the π-conjugated spin systems, 9-anthracen-(3-phenyl-*t*-butylnitroxide) radical (**1*m***) and 9-anthracen-(4-phenyl-*t*-butylnitroxide) radical (**1*p***) systems shown in Fig. 1. These radicals have been designed, and synthesized to clarify the relationship of the photo-excited spin states and π-topology (topology on the delocalized π orbital network). Their photo-excited states have been investigated by time-resolved ESR (TRESR). The spin density distributions provide the most direct information about the spin correlation among the unpaired electrons and the mechanism of the spin alignment in these organic molecules. The mechanism of the intramolecular spin alignment and the role of the spin polarization on the excited states have been discussed based on the spin density distribution calculated by the *ab-initio* molecular orbital calculations. The examples of the direct observations of excited high-spin states (S ≥ 3/2) arising from the radical-triplet pair are still limited [6-17]. They are classified three groups; (I) a stable radical couples weakly with the excited triplet chromophore through sigma bonds[6-9], (II) a stable radical couples weakly by coordination bond [9-13], and (II) a stable radical couples strongly with the chromophore through π-conjugation [14 - 20]. In our previous papers [14 ,15], we reported the first observation of a excited quartet (S = 3/2) state and a quintet (S = 2) state in purely organic π-conjugated spin systems which were generated by a robust spin alignment through π-conjugation between stable iminonitroxide radicals (S = 1/2) and the excited triplet (S = 1) state of a phenyl- or diphenyl- anthracene derivative. In the quintet state, two stable radicals couple through the excited-

Fig. 1 Molecular structures of **1*m*** and **1*p***

[a] *Address here. Division of Molecular Material Science, Graduate School of Science, Osaka City University, 3-3-138 Sugimoto, Sumiyoshi-ku, Osaka 558-8585 (Japan). Fax & Tel: (+81) 6-6605-2559. E-mail: teki@sci.osaka-cu.ac.jp*

Electronic Supplementary Information (ESI) available: [solution ESR spectra, time-profiles of TRESR, spin density distributions in the ground state, details of syntheses and X-ray crystallographic analyses data of **1*m*** and **1*p***]. See DOI: 10.1039/x0xx00000x

triplet-state spin coupler of diphenylanthracene moiety by π-conjugation making a strong exchange interaction possible. In the previous paper [15], we demonstrated that the photo-excited spin states observed by the TRESR were depending on the π-topology. We also clarified the unique excited triplet state generated from four unpaired electrons [18]. Recently, we also reported pentacene derivatives coupled to the stable radical and demonstrated the remarkable photo-stability enhancement due to the enhanced (accelerated) intersystem crossing induced by radical attachment and some contribution of singlet-fission [19, 20]. All of these π-conjugated spin systems, the high-spin photo-excited states were observed for the *para*-joint configuration via phenyl group to the condensed polynuclear aromatic hydrocarbons. This can be well understood taking the spin density distribution in the excited states. However, there is no demonstration of the high-spin excited state for the *meta*-joint configuration. In order to confirm the relationship between π-topology and spin alignment in the photo-excited state, we have designed **1*m*** and **1*p*** for the suitable model systems, in which the excited high-spin state is expected for the *meta*-joint configuration according to the topological rule based on the spin density distribution.

Expected Spin Alignment

It is well established both experimentally and theoretically [21 - 25] that the spin polarization effect plays important role of the spin alignment on the ground state hydrocarbons. It is almost clear that the similar π-topological rule works on the photo-excited states from the studies of the spin alignment on the excited state of the several π-conjugated spin systems [14 - 20]. In the case of iminonitroxide radical systems reported in our previous works, the high-spin (quartet) excited state was detected for the *para*-isomer (**2*p***) and only the doublet low-spin state was observed for the *meta*-isomer (**2*m***). As illustrated by arrows in Fig. 2(a), these results were well understood by taking the spin polarization effect (alternate sign of the spin density between the adjacent carbon atoms) on the phenyl group into account. All of other photo-excited high-spin states in the π-conjugated spin systems reported so far were detected for the similar relationship (*para*-joint configuration via phenyl group between radical moiety and the condensed polynuclear aromatic hydrocarbon moiety). Here, in order to confirm the spin alignment on the photo-excited states and the role of the π-topology, we have designed and synthesized the two novel *t*-butylnitroxide radicals. In their nitroxide radicals, the nitrogen atom links directly to the phenyl group. Therefore, one carbon atom is lacked compared with the iminonitroxide systems. If the spin polarization mechanism works certainly in the spin alignment on the photo-excited state through the phenyl group, *meta*-joint configuration (*meta*-isomer, **1*m***), is expected to have the high-spin quartet excited state as illustrated in Fig. 2(b) together with the spin density distribution (Fig. 2(c)) obtained by *ab-initio* MO molecular orbital calculation and *para*-isomer (**1*p***) has a low-spin doublet state as their lowest photo-excited states. Therefore, the experiments for these *t*-butylnitroxide compounds will give the clear experimental confirmation for the role of the spin polarization in the spin alignment on the photo-excited states.

Fig. 2 Spin alignment in the lowest photo-excited state. (a) **2*p*** in our previous work [15], (b) predicted spin alignment of the quartet excited state of **1*m*** and (c) the calculated spin density distribution of **1*m***.

Results and discussion

UV-vis and Conventional EPR Spectra Typical UV-vis. Spectra of **1*m*** and **1*p*** at room temperature are shown in Fig. 3 in which the characteristic peaks of the anthracene moiety appeared in 300 – 400 nm is slightly red-shifted by ca. 8 nm. These red-shifts are the results of the π-conjugation with the nitroxide radical moiety. An apparent line-broadening of **1*p*** shows that the SOMO (Singly Occupied Molecular Orbital) of the radical moiety in **1*p*** is strongly conjugated with the π-orbital of the phenylanthracene moiety. The typical cw-ESR spectra of **1*m*** and **1*p*** together with their simulations are shown in Fig. S1 (see ESI). The ESR spectra were measured at room temperature using toluene as the solvent. The observed ESR spectra and the spectral simulations of **1*m*** and **1*p*** are shown in Fig. S1 and Fig. S2, respectively. The g values of **1*m*** and **1*p*** were determined to be 2.0065 and 2.0058, respectively. The isotropic hyperfine coupling constants determined from the spectral simulation are summarized in Table 1. From the hyperfine coupling constant the spin densities of the nitrogen atoms of **1*m*** and **1*p*** were determined to be 0.585 and 0.573, respectively, using the McConnell equation ($A_F = Q_N\rho^\pi$, Q_N = 2.11 mT). The hyperfine couplings due to the protons of the pendant phenyl group support the π-conjugation between the SOMO of the nitroxide radical and π-HOMO of the phenylanthracene moiety. The magnitudes of the

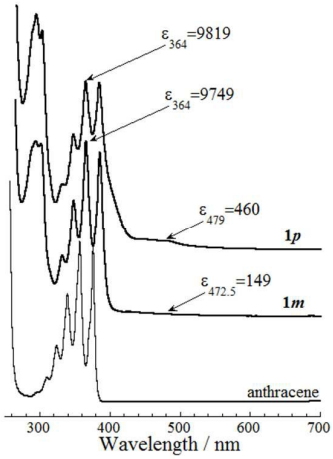

Fig. 3 UV-vis. Absorption spectra **1a**, **1b**, and anthracene at room temperature. EPA was used as their solvent.

hyperfine coupling constants on the phenyl groups and nitrogen atoms show the stronger delocalization of **1*p*** than that of **1*m***.

Table 1 Hyperfine coupling constants determined from the simulation of solution ESR. The hyperfine of *A*(H) = 0.02 mT may come from the proton at 9-proton in the anthracene moiety of **1b**. Other *A*(H)'s were assigned to those of the pendant phenyl groups. *A*(N)'s are the nitrogen atoms in the radical moiety. The Number in the parentheses represents that of the equivalent nuclei.

	A(N) / mT	*A*(H) / mT	*A*(H) / mT	*A*(H) / mT	*A*(H) / mT
1*m*	1.235	0.198 (2)	0.193	0.103	-
1*p*	1.210	0.213	0.210	0.090 (2)	0.020

Photo-Excited Quartet High-Spin State of 1m Typical X-band TRESR spectrum of **1*m*** is shown in Fig. 4. The TRESR spectrum with well-resolved fine structure splitting similar to that of **2*p*** [14, 15] has been observed for **1*m***. An ordinary spin Hamiltonian of a pure spin state (negligible quantum mixing of the different spin states) was used for the analysis:

$$H'_{spin} = \beta_e \boldsymbol{H}.\boldsymbol{g}.S + \boldsymbol{S}.\boldsymbol{D}.\boldsymbol{S}$$
$$= \beta_e \boldsymbol{H}.\boldsymbol{g}.S + D[S_Z^2 - S(S+1)/3] + E(S_X^2 - S_Y^2). \quad (1)$$

The line-shape simulation of the whole spectrum was not reproduced well in this case, although we tried the similar procedures (the eigenfield [21]/exact-diagonalization hybrid method [22] taking the electron spin polarization into account [14]) used for other radical species that reproduced well the whole spectra of the high-spin photoexcited states. In order to determine the spin Hamiltonian parameters, the resonance positions corresponding to the canonical orientations of the fine-structure transitions were calculated by assuming an excited quartet (S = 3/2) state (Q) by the hybrid method. Here, in this assignment of each transition peaks, we assumed E = 0. In the spectrum of Fig. 4, XY peaks become narrow and show a first derivative likes line-shape. Another possibility of the assignment will be discussed in sec. S2 in ESI. Their resonance positions are also shown in Fig. 4 by solid lines with the assignments of the transitions. All canonical resonance fields correspond well to the peak positions of the observed spectrum. The g value and the estimated fine-structure parameters determined from the overall splitting are summarized in Table 2 together with the g-value of the excited doublet state of **1*p***. The magnitude of the D value of **1*m*** is ca.5 % larger than that (0.0235 cm^{-1}) of the quartet state of **2*p***, in which the spin state was determined unambiguously by the simulation of the whole spectrum [14, 15]. In the quartet systems the triplet state of the phenylanthracene moiety couples with the doublet state of the *t*-butylnitroxide by the spin-exchange interaction. In such a exchange-coupled system the wave function of the whole molecule $|\Psi(S, M)\rangle$ is approximately given by the direct product of the wave functions of the two isolated moieties, $|T(S^A, m_A)\rangle$ and $|R(S^B, m_B)\rangle$, as

$$|\Psi(S, M)\rangle = \Sigma\, C(S^A\, S^B\, S;\, m_A\, m_B\, M)\, |T(S^A, m_A)\rangle |R(S^B, m_B)\rangle, \quad \text{for } S^A = 1 \text{ and } S^B = 1/2 \quad (2)$$

where $C(S^A\, S^B\, S;\, m_A\, m_B\, M)$ is the Clebsch- Gordan coefficient. The radical-triplet pair has one quartet and one doublet states. The g and D values for the quartet state (Q) are given by the following relationship [23];

$$g(\mathrm{Q}) = (2/3)g(\mathrm{T}) + (1/3)g(\mathrm{R}), \quad (3)$$
$$g(\mathrm{D}) = (4/3)g(\mathrm{T}) - (1/3)g(\mathrm{R}), \quad (4)$$

and

$$\boldsymbol{D}(\mathrm{Q}) = (1/3)\{\boldsymbol{D}(\mathrm{T}) + \boldsymbol{D}(\mathrm{RT})\}. \quad (5)$$

Here, $\boldsymbol{D}$(T) is the D tensor of the excited triplet moiety, $\boldsymbol{D}$(RT) is the dipolar interaction between the radical spin and the triplet moiety. The estimated g, D and E values calculated using these equations are also summarized in Table 2. In this estimation, g(R) = 2.0065 and g(T) = 2.0040 were used. The D value (0.0710 cm^{-1}) of the excited triplet state of free anthracene was used for D(T) and D(RT) was neglected. The experimentally determined g, D and E values for the excited quartet state are in excellent agreement with the calculations.

The 5 % increase of the D value is reasonable magnitude because the average distance between the radical site and the excited triplet part of the anthracene moiety becomes shorten by the lack of one linking carbon site compared with the iminonitroxide systems. An estimation of the dipolar interaction term supported this result. The well agreement of all the canonical resonance fields between the observed spectrum and the calculated ones under the assumption of S = 3/2 and the reasonable magnitude of the D value show that the observed excited state of **1*m*** is a quartet high-spin state, in which is generated by the spin alignment between the excited triplet of phenylanthracene moiety and the pendant radical spin. The direct observations of the excited quartet state show that the photoinduced intramolecular spin alignment is realized between the excited triplet state (S =1) of the phenylanthracene moiety and the doublet spin (S =1/2) of the pendant radical as illustrated in Fig. 2(b).

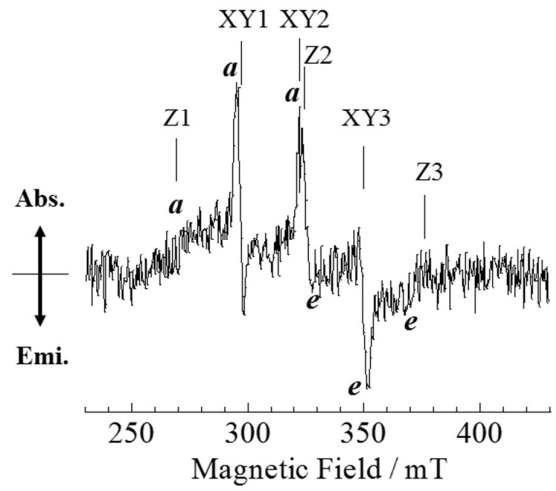

Fig. 4 Typical TRESR spectrum of **1*m*** at 25 K in EPA frozen glass matrix detected at 0.6 μs after pulsed LASER excitation. *a*/*e* means the absorption/emission of the microwave. The observed microwave frequency is 9.06848 GHz. The solid lines show the canonical resonance field positions corresponding to the XYZ principal axes of the fine-structure tensor. The calculated canonical resonance fields and the *a*/*e* properties are Z1(269.78 mT, *a*), XY1(296.57 mT, *a*), XY2(321.55 mT, *a*), Z2(323.21 mT, no intensity), XY3(349.81 mT, *e*), and Z3(376.64 mT, *e*), respectively.

Table 2 g values and the fine-structure parameters determined from the calculations of the canonical resonance fields. The values in parentheses are estimated values using eqs. (3) – (5).

	S	*g* value	D / cm^{-1}	E / cm^{-1}
1*m*	3/2	2.005 (2.004$_8$)	0.0250 (0.0237)	0.0
1*p*	1/2	2.003 (2.003$_2$)	-	-

Doublet Low-Spin State of 1p observed by TRESR In the phnylanthracene-iminonitroxide and diphenylanthracene-bis (imononitroxide) systems the photo-excited states detected by the TRESR experiments were drastically changed depending on the π-topology [14,15,18]. These phenomena were well understood by assuming that the lowest photo-excited states were observed in the TRESR experiments and taking the spin polarization effect on the phenyl groups into account on the photo-excited states. Ab-initio molecular orbital calculations of the lowest photo-excited states supported theoretically this finding. In order to give the further experimental test about the role of the π-topology in the spin alignment, TRESR experiments were performed for the π-topological isomer, **1*p***. In contrast to the result of **1*m***, no TRESR signal attributable to the high-spin excited state was observed for **1*p*** and only a weak absorptive signal due to the doublet state was observed as shown in Fig. 5. There is two possibility of this doublet signal, (1) the photo-excited doublet state arising from the exchange coupled doublet spin state between the triplet state of anthracene moiety and the radical spin, and (2) the doublet ground state spin-polarized through the photo-excited states. In order to obtain the more information, we compared that the integrated cw-ESR spectrum and the TRESR spectrum (Fig. S4 in ESI). The comparison indicates that the TRESR spectrum is not same as the integrated cw-ESR spectrum. Fig. S4(c) shows that the TRESR signal has a slight smaller g value than that of the ground-state and/or at least the signal with a little smaller g-value is overlapped to the ground doublet signal. In addition, the sign inversion expected for the ground-state doublet signal [24] was not observed (see Fig. S5 in ESI), although it is difficult to say conclusively because of the weak signal intensity. Thus, a drastic change of the photo-excited spin state detected by the TRESR experiment was also observed. This agrees with the π-topological rule, indicating that the lowest excited state of **1*p*** is a low-spin doublet (S = 1/2) spin state and the sign of the intramolecular exchange is antiferromagnetic [14, 15, 25].

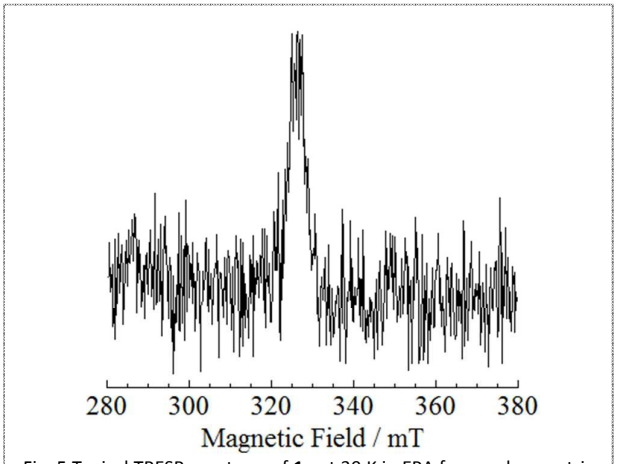

Fig. 5 Typical TRESR spectrum of **1*p*** at 30 K in EPA frozen glass matrix detected at 0.6 μs after pulsed LASER excitation. The observed microwave frequency was 9.1571 GHz. The signal shows microwave absorption.

These findings give the clear demonstration that the sign of the intramolecular exchange interaction and the spin multiplicity of the lowest photo-excited spin-state change drastically depending on the topological nature of π-electron network. Thus, the π-topological rule of the spin polarization established for the ground states of the aromatic hydrocarbons also plays an important role in the spin alignment on the excited states. This finding will be supported by the theoretical calculation using the spin density distributions obtained using the *ab*-initio molecular orbital calculations as described latter.

ESP in the Photo-Excited Quartet State of 1m In the iminonitroxide system, **2*p*** [14,15], the relative population of the zero-field spin sublevels on the quartet states can be interpreted by assuming the selective intersystem crossing to Ms' = ±1/2 spin sublevels, which are generated by spin-orbit coupling between the excited doublet states and the eigenfunctions of the excited quartet state in zero magnetic field. The origin of the selective ISC was attributed to the enhanced ISC mechanism which was caused by the attachment of the localized doublet radical [15]. Although the quartet TRESR spectrum of **1*m*** could not reproduce the whole line-shape well by the spectral simulation, the pattern of the spectrum is similar to that of **2*p***. Thus, the spectra of **1*m*** shows the *aaa*/*eee* pattern in the low-field/high-field regions (*a* and *e* are absorption and emission of the microwave, respectively), which is similar to that of the quartet TRESR spectrum of **2*p***. Therefore, it is clear that the dynamic electron spin polarization is dominantly generated by the selective intersystem crossing to Ms' = ±1/2 zero-field spin sublevels of the quartet state. The origin of the line-width narrowing at the XY canonical orientations of the fine-structure tensor is unknown, although it seems to be caused by the some dynamical process. The time profiles for the TRESR signals of **1*m*** and **1*p*** at typical canonical resonance position of the fine-structure tensor are shown in Fig. S6 in ESI.

Mechanism of Spin Alignment

The mechanism of the spin alignment was clarified based on the spin density distribution. In the excited quartet state the

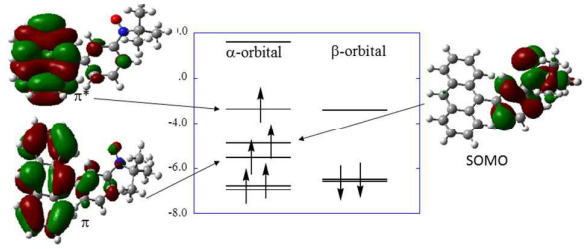

Fig. 6 Energy levels of the excited quartet state of **1*m*** and the one-electron molecular orbitals occupied by the unpaired electrons.

spin density distribution of the anthracene moiety is nearly symmetrical as shown in Fig. 2(c). The almost two net unpaired spins exist in the anthracene moiety and the one unpaired spin exists on the radical moiety. Fig. 6 shows the energy levels and the one-electron molecular orbitals occupied by the unpaired electrons. This shows that the excited quartet state is generated by the one-electron transition from the β–NHOMO (π) to the α-LUMO (π*). These results are consistent with our experimental results, in which the magnitude of the observed fine-structure splitting has been well interpreted as the exchange coupled system constructed from the ππ* excited triplet state of anthracene and the pendant radical. In the anthracene moiety, spin delocalization occurs. In contrast, the alternating sign of the spin density is realized on the phenyl groups as shown in Fig. 2(c). This sign alternation of the spin densities shows that the spin polarization mechanism overcomes the spin delocalization within the dangling phenyl groups even in the excited state. Thus, through the spin polarization in the phenyl group, the unpaired spin on the radical moiety couples ferromagnetically to the excited triplet spins delocalized on the anthracene moiety, leading to the excited quartet high-spin state.

Decay Profiles of Excited States of 1m and 1p

It is difficult to estimate the life times of the phtoexcited states of **1*m*** and **1*p*** from the time profiles of the TRESR, because the intensities of the TRESR signals decrease both the spin-lattice relaxation and the life-times of the excited states. Therefore, we carried out the transient absorption measurements. Fig. 7 shows the decay of the transient absorption signals in the frozen glass matrix at 77 K, which are attributed to the photo-excited triplet state of the phenylanthracene moiety. The decay profiles were well analysed by double exponential fits. In the case of **1*m***, the double exponential fit was apparently better than the single exponential fit. The better fitting was also obtained for **1*p*** using the double exponential function, although the decay could be analysed by the single exponential function. The parameters obtained by the analyses are summarized in Table 3. The double exponential fits is reasonable because there are one doublet state and one quartet state generated by a intersystem crossing of the phenylanthracene moiety. In such a case, the decays should be the double exponential because there are pathways from the quartet state to the doublet state and the vice versa [26] and the both states gives the transient absorption signals arising from the triplet excited state of the phenylanthracene moiety that can be not distinguished to each other (see sec.S7 in ESI). The comparison of the data of **1*m*** and **1*p*** shows that the contribution of the component with longer life time of **1*m*** is larger than that of **1*p***. This is consistent with the energy location expected from the topological rule of the spin alignment that the quartet state with the low-lying higher energy doublet state is the lowest photoexcited state of **1*m*** and the doublet state with the higher energy quartet state is that of **1*p***. In the TRESR spectra, dominantly quartet state was observed in **1*m*** and the doublet state in **1*p***, although their transient absorption signals show the double exponential decays in both cases. This is not the contradiction. It should be noted that the signal intensity of the TRESR comes from the dynamic electron spin polarization generated due to the anisotropic intersystem crossing among the spin sublevels. Thus, the mechanism leading not the difference of the spin sublevels gives no dynamic electron spin polarization, leading to weak intensity of TRESR signal. The thermal excitation from the lower energy spin state to the low-lying higher energy spin state is such an example. Therefore, the decay pathway via the low-lying doublet state from the lowest quartet excited state leads to the double exponential decay of the transient absorption signal but the signal populated during the pathway by the thermal excitation is difficult to be detected by TRESR. A similar situation occur the decay from the lowest doublet excited state. The present situations of **1*m*** and **1*p*** can be understood as such cases.

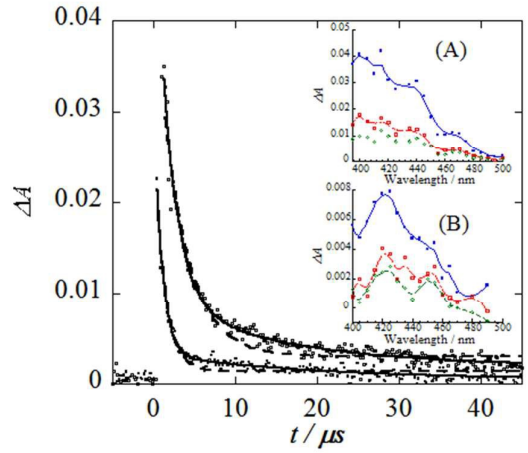

Fig. 7 Decay profiles of the intensities of the transient absorption spectra of **1*m*** and **1*p*** at 77 K in the frozen EPA glass matrix. Upper and lower ones are the decays of **1*m*** and **1*p***, respectively. Solid line is the least square fit using double exponential functions. Broken line is a single exponential fit. (A) and (B) are the transient absorption spectra of **1*m*** and **1*p***, respectively. The plots is observed data and lines are sommzed ones. Blue, red, and green ones correspond to the data at 2 μs, 4 μs, and 6 μs after the photoexcitation, respectively.

Table 3 Decay times determined from the time profiles of the transient absorption signals. For he double and single exponential fittings, the following equations were used.

$\Delta A(t) = B1 \exp(-t/\tau 1) + C1 \exp(-t/\tau 2)$, (6)

$\Delta A(t) = B2 \exp(-t/\tau 3)$ (7)

	Double Exp. Fit.				Single Exp. Fit.	
	B1	*τ1/μs*	*C1*	*τ2/μs*	*B2*	*τ3/μs*
1*m*	0.046	1.93	0.008	14.9	0.040	3.3
1*p*	0.028	0.96	0.003	19.7	0.026	1.3

Experimental

3.1 Materials **1*m*** and **1*p*** were synthesized according to the procedures shown in Scheme 1(a) and 1(b), respectively. The details of the synthetic procedures are described in the ESI. Samples were purified by the column chromatography on alumina (Merk

Aluminium Oxide 90) with CH_2Cl_2 and by re-crystallization from EtOH. **1*m*** and **1*p*** were obtained as dark red needles. (**1*m***: Found: C, 84.51; H, 6.86; N, 4.02. **1*p***: Found: C, 84.20; H, 6.52; N, 4.04. $C_{24}H_{22}NO$ requires: C, 84.67; H, 6.51; N, 4.11). Their molecular structures determined by X-ray crystallographic analyses are given in ESI.

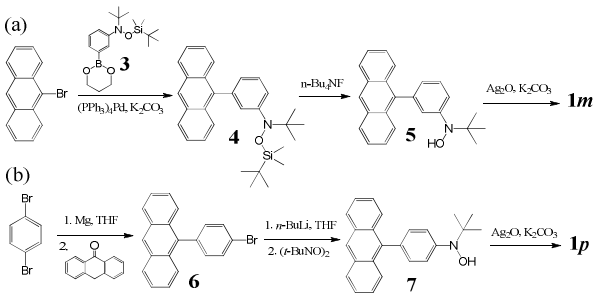

Scheme 1 Synthetic procedures of **1*m*** and **1*p***.

3.2 Measurements Conventional cw-ESR was measured by a JEOL-TE300 X-band ESR spectrometer with an Oxford ESR 910 cold He gas flow system and optical absorption spectra were taken at room temperature on the conventional UV-vis. Spectrometer (Hitachi-U3000). The conventional cw-ESR spectra with the hyperfine-splitting in solution were analysed by a spectral simulation according to the ordinary method. TRESR experiments were carried out at 30 K using JEOL-TE300 X-band ESR spectrometer. Transient ESR signals from the detector diode were amplified by a wideband preamplifier and accumulated using a high-speed digital oscilloscope (LeCroy 9350C). Excitation was carried out at 355 nm light by a Nd:YAG ns pulse laser (Continuum Surelite II-10). EPA (diethylether : isopentane : ethanol = 5 : 5 : 2) glass matrix was used for all TRESR experiments. Samples were degassed by repeated freeze-pump-thaw cycles using a high vacuum lime system. Transient absorption spectra were measured at 77 K using home-made system with an Oxford OptistatCF, the above pulse laser, a monochromater (JASCO CT-25C) followed by a photomultiplier (Hamamatsu R1221), cw Xe lamp (USHIO) and the above high-speed oscilloscope.

3.3 Molecular Orbital Calculation In order to obtain the physical picture of the photo-induced intramolecular spin alignment, the ab-initio molecular orbital calculations were carried out based on the density functional theory (DFT) using Gaussian 98 [27]. In these calculations, an unrestricted Hartree-Fock method (Ubecke 3LYP/6-31G) was employed in order to clarify the role of the spin polarization effect.

Conclusions

The photo-excited spin states and their spin alignment of phenylanthracene-*t*-butylnitroxide radical systems, **1*m*** and **1*p***, are synthesized and investigated by TRESR and transient absorption experiments and *ab-initio* MO calculations. Role of the spin delocalization and the spin polarization effects are revealed in the spin alignment on the excited states. The photo-induced spin alignments were achieved through the photo-excited triplet spin couplers. π-Topology plays very important role on the spin alignment on the photo-excited states as well as the ground states. The π-topological rules of the spin alignment on the photo-excited states was confirmed in this work.

Acknowledgements

Authors acknowledge to Dr. Satoru Nakajima for his help of the setup of the transient absorption apparatus and Dr. Rika Tanaka(Analytical Center of Osaka City University) for her X-ray crystallographic analyses. This work was the financial support mainly by the Grant-in-Aid for Scientific Research (mainly No. 13440211) by from the Ministry of Education, Science, Sports and Culture, Japan.

Notes and references

1 For an overview of molecule-based magnetism see: G. Christou ed., *Polyhedron* (Special Issue of ICMM2012), 2013, **66**, 1-298.
2 For an overview of organic spintronics see: W. Gillin and N. Morley ed., *Synthetic Metals* (Special Issue of SPINOS2012), 2013, **173**, 1-56.
3 (a) M. Matsushita, H. Kawakami, Y. Kawada and T. Sugawara, *Chem. Letters*, 2007, 110. (b) M. Matsushita, H. Kawakami, T. Sugawara and M. Ogata, Phys. Rev., 2008, **B77**, 195208.
4 (a) O. Sato, J. Tao and Y.-Z. Zhang, *Angew. Chem*., 2007, **119**,2200, (*Angew. Chem., Int. Ed*., 2007, **46**, 2152) and references cited therein. (b) D. A. Shultz, in Magnetism: Molecules to Materials II, ed. J. S. Miller and M. Drillon, Wiley-VCH, Weinheim, 2001, p. 281.
5 (a) Y. Teki, *Polyhedron*, 24, 2299. (b) K. Katayama, M. Hirotsu, I. Kinoshita and Y. Teki, *Dalton Trans*, 2012, **41**, 13465.
6 C. Corvaja, M. Maggini, M. Prato, G. Scorrano and M. Venzin, *J. Am. Chem. Soc.* 1995, **117**, 8857.
7 J. Fujiwara, Y. Iwasaki, Y.Ohba, S. Yamauchi, N. Koga, S. Karasawa, M. Fuhs and K. Möbius, S. Weber, *Appl. Magn. Reson*. 2001, **21**, 483, and references therein.
8 M. T. Colvin, E. M. Giacobbe, B. Cohen, T. Miura, A. M. Scott and M. R. Wasielewski, *J. Phys. Chem. Soc*. 2010, **114**, 1741.
9 K. Ishii, J. Fujiwara, Y. Ohba and S. Yamauchi, *J. Am. Chem. Soc*. 1996, **118**, 13079.
10 K. Ishii, Y. Hirose and N. Kobayashi, *J. Phys. Chem*. 1999, **103**, 1986, and references cited therein.
11 M. Asano-Someda, A. van der Est, U. Kru¨ger, D. Stehlik, Y. Kaizu and H. Levanon, *J. Phys. Chem. A* 1999, **103**, 6704.
12 A. van der Est, M. Asano-Someda, P. Ragogna and Y. Kaizu, *J. Phys.Chem. A* 2002, **106**, 8531.
13 P. K. Poddutoori, M. Pilkington, A. Alberola, V. Polo, J. E. Warren and A. van der Est, *Inorg.Chem.* 2010, **49**, 3516, and references cited therein
14 Y. Teki, S. Miyamoto, K. Iimura, M. Nakatsuji and Y. Miura, *J. Am. Chem. Soc*. 2000, **122**, 984.
15 Y. Teki, S. Miyamoto, K. Iimura, M. Nakatsuji and Y. Miura, *J. Am. Chem. Soc*. 2001, **123**, 294.
16 Y. Teki, M. Nakatsuji and Y. Miura, *Mol. Phys*. 2002, **100**, 1385.
17 Y. Teki, M. Kimura, S. Narimatsu, K. Ohara and K. Mukai, *Bull. Chem. Soc. Jpn*., 2004, **77**, 95.
18 (a) Y. Teki and S. Nakajima*, Chem. Lett*. 2004, **33**, 1500; (b) Y. Teki, T. Toichi and S. Nakajima*, Chem. Eur. J.* 2006, 12, 2329.
19 (a) Y. Teki, H. Tamekuni, J. Takeuchi and Y. Miura, *Angew. Chem. Int. Ed.,* 2006, **45**, 4666; (b) Y. Teki, H. Tamekuni, K. Haruta, J. Takeuchi and Y. Miura, *J. Mater. Chem.* 2008, **18,** 381.

20 (a) Y. Kawanaka, A. Shimizu, T. Shinada, R. Tanaka and Y. Teki, *Angew. Chem. Int. Ed.,* 2013, **52**, 6643; (b) A. Ito, A. Shimizu, N. Kishida, Y. Kawanaka, D. Kosumi, H. Hashimoto and Y. Teki, *Angew. Chem. Int. Ed.,* 2014, **53**, 6715.

21 G. G. Belford, R. L. Belford, J. F. Bukhalter, *J. Magn. Reson.* 1973, **11**, 251.

22 Y. Teki, I. Fujita, T. Takui, T. Kinoshita, and K. Itoh, *J. Am. Chem. Soc*. 1994, **116**, 11499.

23 A. Bencini and D. Gatteschi, *EPR of Exchange Coupled Systems*, Springer-Verlag, Heidelberg, 1990.

24 J. Fujiwara, K. Ishii, Y. Ohba, S. Yamauchi, M. Fuhs, and K. Möbius, *J. Phys. Chem. A*, 1997, **101**, 5869.

25 I. Confini, P. P. Lainé, M. Zamboni, C. A. Daul, V. Marvaud and C. Adamo, *Chem. Eur. J.*, 2007, **13**, 5360.

26 M. Asano, Y. Kaizu and H. Kobayashi, *J. Chem. Phys*., 1988, **89**, 6567.

27 Gaussian 98, Revision A.11, M. J. Frisch, G. W. Trucks, H. B. Schlegel, G. E. Scuseria, M. A. Robb, J. R. Cheeseman, V. G. Zakrzewski, J. A. Montgomery, Jr., R. E. Stratmann, J. C. Burant, S. Dapprich, J. M. Millam, A. D. Daniels, K. N. Kudin, M. C. Strain, O. Farkas, J. Tomasi, V. Barone, M. Cossi, R. Cammi, B. Mennucci, C. Pomelli, C. Adamo, S. Clifford, J. Ochterski, G. A. Petersson, P. Y. Ayala, Q. Cui, K. Morokuma, P. Salvador, J. J. Dannenberg, D. K. Malick, A. D. Rabuck, K. Raghavachari, J. B. Foresman, J. Cioslowski, J. V. Ortiz, A. G. Baboul, B. B. Stefanov, G. Liu, A. Liashenko, P. Piskorz, I. Komaromi, R. Gomperts, R. L. Martin, D. J. Fox, T. Keith, M. A. Al-Laham, C. Y. Peng, A. Nanayakkara, M. Challacombe, P. M. W. Gill, B. Johnson, W. Chen, M. W. Wong, J. L. Andres, C. Gonzalez, M. Head-Gordon, E. S. Replogle, and J. A. Pople, Gaussian, Inc., Pittsburgh PA**, 2001.**

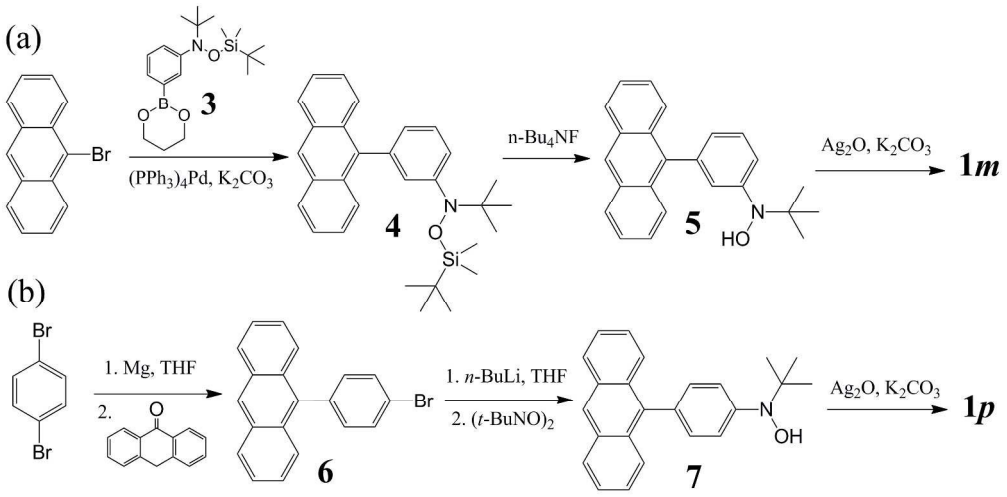

253x125mm (300 x 300 DPI)

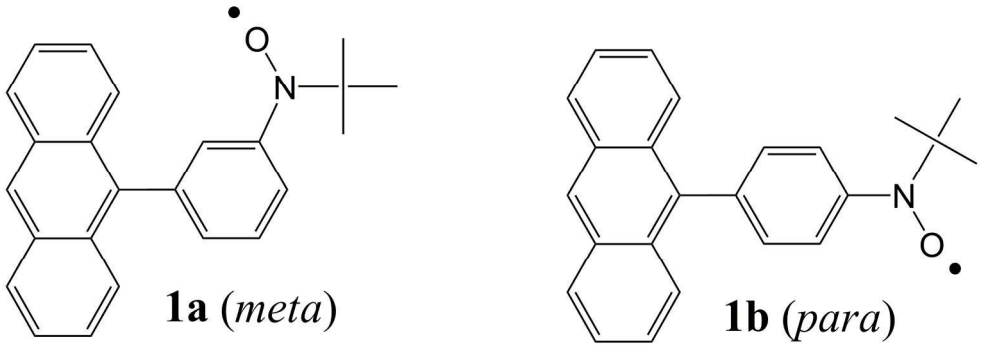

590x207mm (96 x 96 DPI)

Figure 2 (Teki et al., π-Topology and Spin Alignment in the Photo-Excited States...)

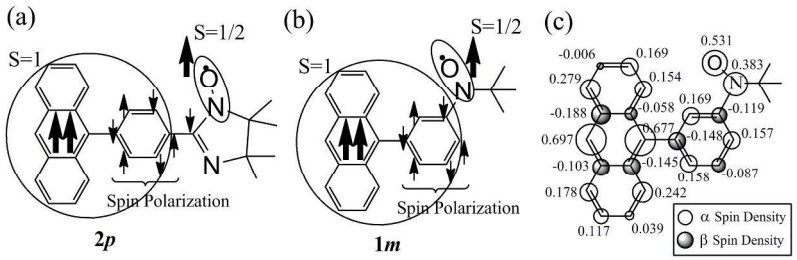

245x106mm (300 x 300 DPI)

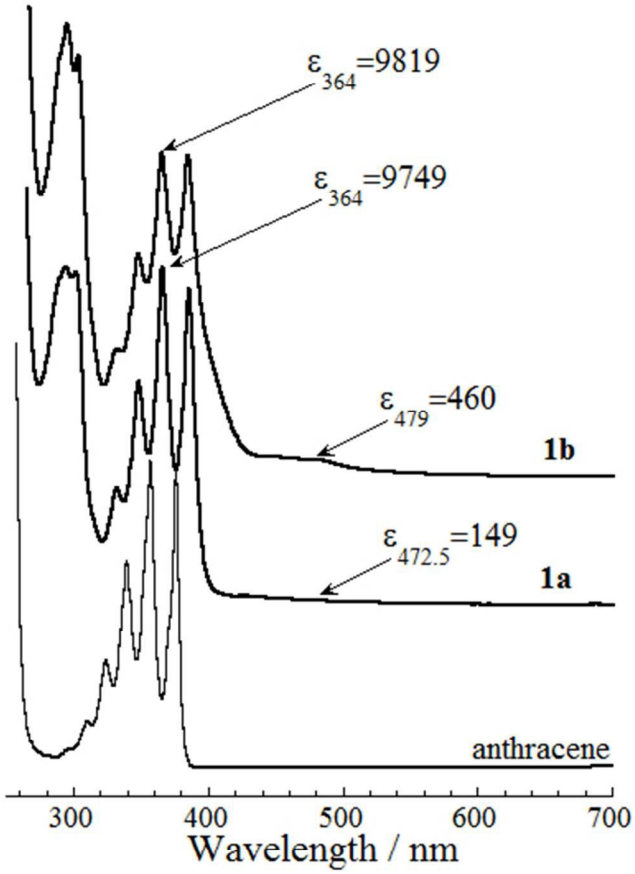

194x257mm (72 x 72 DPI)

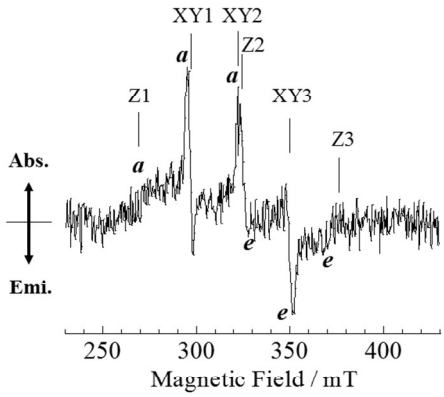

338x190mm (96 x 96 DPI)

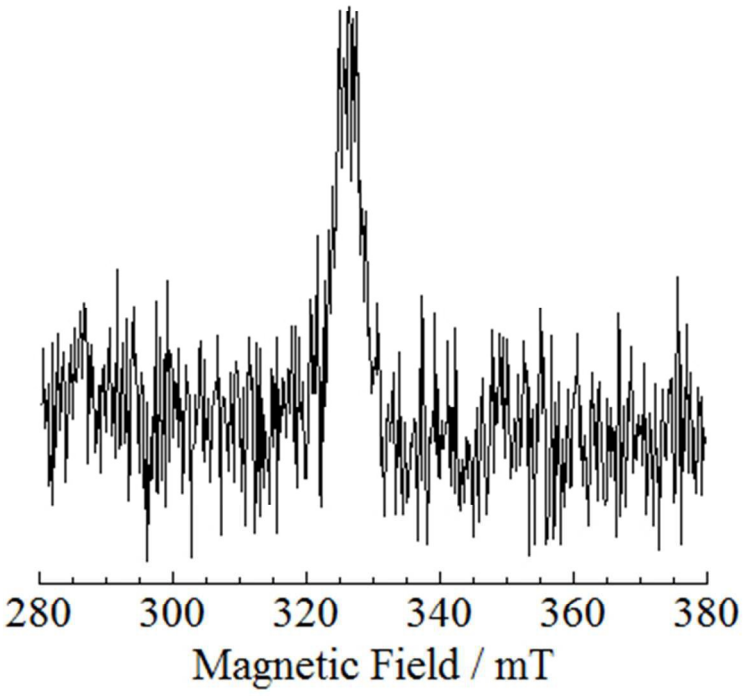

190x169mm (72 x 72 DPI)

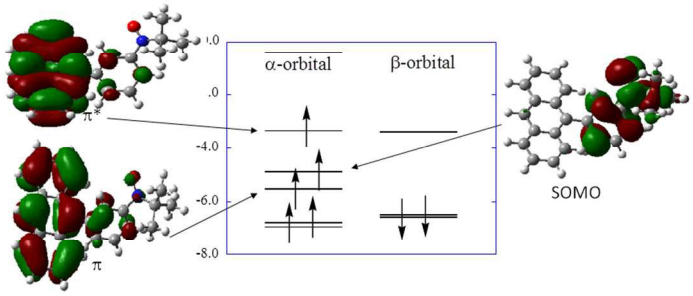

338x190mm (96 x 96 DPI)

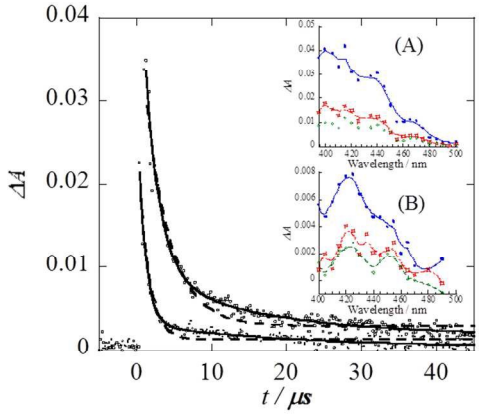

338x190mm (96 x 96 DPI)